npj | computational materials

Article

Published in partnership with the Shanghai Institute of Ceramics of the Chinese Academy of Sciences

https://doi.org/10.1038/s41524-024-01344-0

First-principles predictions of HfO_2-based ferroelectric superlattices

Binayak Mukherjee [1] ✉, Natalya S. Fedorova[1] & Jorge Íñiguez-González [1,2] ✉

The metastable nature of the ferroelectric phase of HfO_2 is a significant impediment to its industrial application as a functional ferroelectric material. In fact, no polar phases exist in the bulk phase diagram of HfO_2, which shows a dominant non-polar monoclinic ground state. As a consequence, ferroelectric orthorhombic HfO_2 is stabilized either kinetically or via epitaxial strain. Here, we propose an alternative approach, demonstrating the feasibility of thermodynamically stabilizing polar HfO_2 in superlattices with other simple oxides. Using the composition and stacking direction of the superlattice as design parameters, we obtain heterostructures that can be fully polar, fully antipolar or mixed, with improved thermodynamic stability compared to the orthorhombic polar HfO_2 in bulk form. Our results suggest that combining HfO_2 with an oxide that does not have a monoclinic ground state generally drives the superlattice away from this non-polar phase, favoring the stability of the ferroelectric structures that minimize the elastic and electrostatic penalties. As such, these diverse and tunable superlattices hold promise for various applications in thin-film ferroelectric devices

Originally studied as a high-permittivity dielectric with commercial applications in the mass production of complementary metal-oxide-semiconductors (CMOS), it is only relatively recently that HfO_2 has been established as a ferroelectric (FE), with the first reports appearing in 2011[1,2]. Subsequently, FE HfO_2 has become the subject of intense research interest – not just for its CMOS-compatibility and associated technological promise, but also for the atypical origin and nature of ferroelectricity in this fluorite-structured simple oxide. Multiple theoretical models have been proposed[3–6], suggesting both an improper[3] and proper[4,5] nature of ferroelectricity, with recent experimental results favoring the latter[7]. The piezoresponse of HfO_2 is just as peculiar, displaying a potentially tunable[8] longitudinal piezoelectric effect whose sign is non-trivial[9–12].

The ground state for bulk HfO_2 at room temperature and pressure is the monoclinic "m" phase (space group $P2_1/c$, Fig. 1a). At 1973 K, it transitions into the tetragonal "t" phase ($P4_2/nmc$, Fig. 1b), and then at 2773 K into the cubic "c" phase ($Fm\text{-}3m$, Fig. 1c). With increasing pressure instead, the m phase transitions into an antipolar orthorhombic "oI" phase ($Pbca$, Fig. 1d), and then into a different orthorhombic "oII" phase ($Pnma$). The polar phases, which do not appear in the bulk phase diagram, include the rhombohedral ($R3m$) and orthorhombic "oIV" ($Pmn2_1$) states, as well as the most common ferroelectric orthorhombic "oIII" phase ($Pca2_1$, Fig. 1e)[1]. The polarization in this oIII phase is quite distinct from that in ferroelectric perovskites and can be visualized as an off-centering of half the oxygens (which we will call "polar" or "active" oxygens in the following, marked by blue arrows in Fig. 1e) in the unit cell, with respect to the high-symmetry positions they occupy in the cubic structure[13]. By contrast, the other half of the oxygens ("spacer" or "buffer" oxygens in the following, dashed box in Fig. 1e) remain close to their high-symmetry positions and do not contribute significantly to the polarization. The oIII phase presents an oxygen coordination of 7 for each cation (3 polar and 4 buffer), as described by the so-called 7 C theory of ferroelectricity in HfO_2, which claims that this unusual coordination number serves as a fingerprint of ferroelectricity in simple oxides and halides[14]. A closely related polymorph of interest is the higher energy antipolar "o-AP" phase ($Pbcn$, Fig. 1f), where we may say that the buffer oxygens undergo an off-centering equal and opposite to that of the polar oxygens (dashed box and green arrows in Fig. 1f). This phase is one among several proposed paraelectric reference structures to discuss ferroelectricity in the oIII phase[4,5], but – as far as we know – has never been observed experimentally in bulk HfO_2.

The stabilization of the metastable FE oIII phase has been attributed to a multitude of factors, including oxygen vacancies, dopant species and concentration, surface energy minimization, quenching kinetics, and mechanical effects[15]. In fact, both conventional nucleation theory[16] as well as atomistic nudged elastic band (NEB) calculations using density functional theory (DFT)[17,18] suggest that the oIII phase is stabilized kinetically over the m phase, which is the thermodynamic ground state. Recent first-principles results suggest an alternate mechanism where specific epitaxial conditions can thermodynamically favor the ferroelectric o-III phase over the m phase in <111 > -oriented films[19]. As such,

[1]Department of Materials Research and Technology, Luxembourg Institute of Science and Technology (LIST), Esch-sur-Alzette, Luxembourg. [2]Department of Physics and Materials Science, University of Luxembourg, Belvaux, Luxembourg. ✉e-mail: binayak.mukherjee@list.lu; jorge.iniguez@list.lu

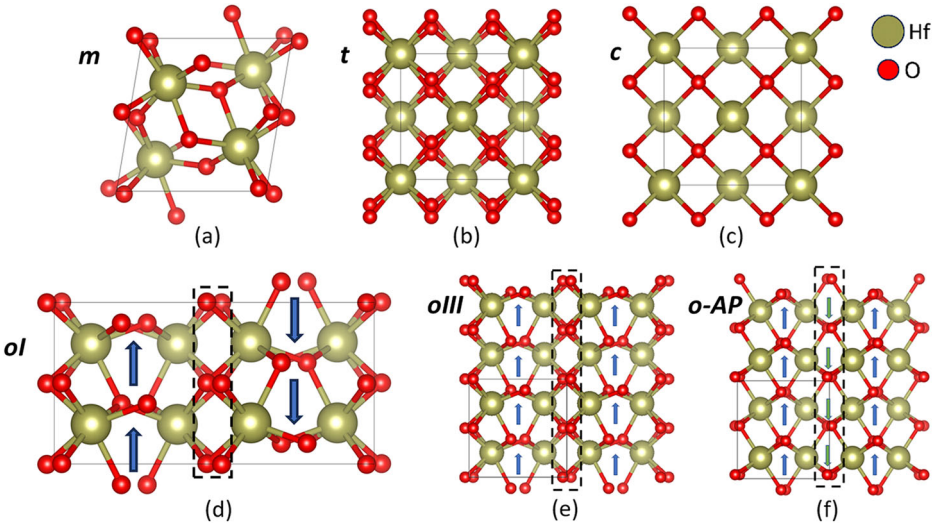

Fig. 1 | Polymorphs of HfO_2. Some relevant polymorphs of HfO_2, including the (**a**) monoclinic, (**b**) tetragonal, (**c**) cubic, (**d**) orthorhombic-I, (**e**) orthorhombic-III, and (**f**) orthorhombic-AP phases. The phase label is given in the top left corner of each structure. The arrows indicate the direction of the local dipoles in each half unit cell, taking the cubic phase (**d**) as reference; the dashed boxes identify the so-called "spacer layers".

replacing the monoclinic structure with a polar ground state, particularly in <100 > -oriented films, remains an open problem.

A promising way forward is through the design of nanostructures that may allow us to achieve that goal. One such candidate nanostructure is a superlattice (SL), i.e., a periodic lattice consisting of nanometric layers of two different materials. DFT calculations have shown that Si dopants in oIII HfO_2 adopt stable, layered configurations akin to SLs, and lead to a ferroelectric oIII ground state[20]. Recent reports on ZrO_2/HfO_2 (Zr/Hf) SLs demonstrate enhanced polarization, improved reliability at high temperatures, a tunable coercive field[21] and high stability of the ferroelectric state[22]. Such superlattices have recently been used as gate dielectrics in transistors[23] and to obtain wake-up free ferroelectric capacitors[24]. Despite the heightened interest, the mechanism behind the formation of the oIII phase in the superlattices is not fully understood, though some propose that it is connected to the in-plane tensile strain at the interface[25]. A DFT study has also suggested that the enhanced endurance of these FE SL's can be explained by a suppression of oxygen vacancies[26].

The promising results obtained for Zr/Hf SLs naturally justify an interest in similar heterostructures with other simple oxides. Yet, such studies are conspicuous by their absence, a situation which the present work seeks to partially remedy. Here we report our DFT results on superlattices of HfO_2 with a series of simple oxides, predicting that we can thus stabilize ground state phases with polar, antipolar, and mixed polar/antipolar or polar/nonpolar characters. Our results lend themselves to a simple interpretation in terms of elastic and electrostatic considerations, and allow us to identify the most promising directions for the growth of ferroelectric HfO_2-based superlattices

Results

Pure compounds

To explore the behavior of the SL's, we first consider the bulk structures of the pure compounds. Apart from HfO_2, we choose all the other group IV (A and B) oxides, as well as the fluorite structured lanthanide CeO_2. These are all simple compounds with the chemical formula XO_2, where X is a 4+ cation (X = Si, Ge, Ti, Sn, Zr, Pb and Ce, in increasing order of cation radius, Table 1). They are mostly ionic in nature with large band gaps. Starting from geometries isostructural to the oIII, oI, m and t phases of HfO_2, each pure compound is fully relaxed to determine the relative stability of such polymorphs, leading to an interesting structural classification.

It is noteworthy that *only* HfO_2 and ZrO_2 are found to have ground states in the centrosymmetric m phase, whereas for SiO_2, GeO_2, SnO_2 and PbO_2 neither the m phase nor the oIII phase are stable. Starting from either of these phases and minimizing the Hellmann-Feynman forces and total

Table 1 | The chosen oxides, their cation radii[41], selected polymorphs considered in this work, and their corresponding energies relative to their respective ground state

Oxide	Cation radius (Å)	*Space group* (phase label)	Energy (meV/cation)
SiO_2	0.4	*I-42d*	0
		Pbcn (o-AP)	346
		$P4_2/nmc$ (t)	702
		Pbca (oI')	1335
GeO_2	0.53	$P4_2/mnm$	0
		Pbcn (o-AP)	98
		$P4_2/nmc$ (t)	618
		Pbca (oI')	742
TiO_2	0.74	*Pbcn* (o-AP)	0
		$P2_1/c$ (m)	28
		Pbca (oI)	158
		$Pca2_1$ (oIII)	172
		$P4_2/nmc$ (t)	278
SnO_2	0.81	$P4_2/mnm$	0
		Pbcn (o-AP)	49
		Pbca (oI)	329
		$P4_2/nmc$ (t)	433
HfO_2	0.83	$P2_1/c$ (m)	0
		Pbca (oI)	46
		$Pca2_1$ (oIII)	**64**
		Pbcn (o-AP)	127
		$P4_2/nmc$ (t)	139
ZrO_2	0.84	$P2_1/c$ (m)	0
		Pbca (oI)	41
		$Pca2_1$ (oIII)	52
		$P4_2/nmc$ (t)	79
PbO_2	0.94	*Pbcn* (o-AP)	0
		Pbca (oI)	56
		$P4_2/nmc$ (t)	102
CeO_2	0.97	*Fm-3m*	0

The energy of oIII HfO_2 is hilighted in bold.

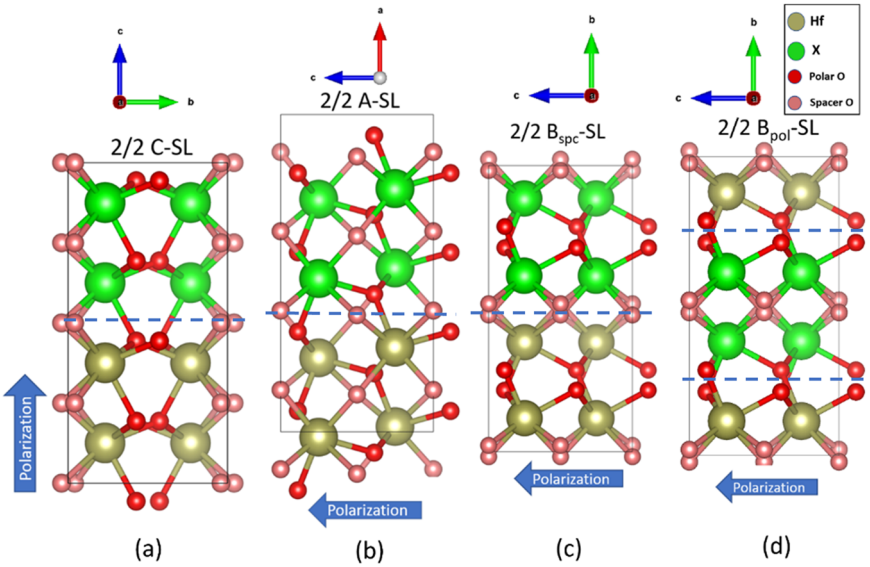

Fig. 2 | Structures of the considered 2/2 X/Hf oIII SL's superlattices. (**a**) stacking in the C-direction (parallel to polarization), (**b**) stacking in the A-direction (perpendicular to polarization, mixed interface), (**c**) stacking in the B-direction (perpendicular to polarization, spacer interface), and (**d**) stacking in the B-direction (perpendicular to polarization, polar interface). Dashed line demarcates the interface.

energy causes the systems to relax into the centrosymmetric antipolar o-AP structure (Fig. 1f). This structure is also the ground state for PbO_2[27] and TiO_2[28], with the latter additionally having local minima corresponding to the m and oIII phases. GeO_2 and SnO_2 have ground states in the structurally similar tetragonal rutile $P4_2/mnm$ phase[29,30], while the ground state for SiO_2 has been proposed to be the tetragonal $I\text{-}42d$ phase[31]. The oI phase, which is the preferred antipolar configuration for HfO_2 and ZrO_2, also exists as a high energy state in the other oxides, though in a distorted form (oI') in SiO_2 and GeO_2 (see Supplementary Note S1), alongside higher energy tetragonal phases. Finally, we have the peculiar case of CeO_2, which strongly favors a ground state in the fluorite c phase and relaxes to that structure regardless of the starting geometry, again suggesting the absence of any oIII or m local minima.

Computational approach for the superlattices

For the purposes of this study, we construct SLs with infinitely repeating, alternating layers of HfO_2 and XO_2. Unless otherwise indicated, in our simulations the starting geometries for the SLs are the same for both layers, and four separate polymorphs are considered: the polar oIII phase, and the centrosymmetric oI, m, and t phases. The initial structures are allowed to relax fully, without imposing any epitaxial conditions. (This would correspond to free-standing or fully-relaxed films in experiments.) Two layer thicknesses are considered, with either 2 or 4 cation sublayers in each layer, denoted as 2/2 and 4/4 SLs respectively. The SLs are stacked along the pseudo-cubic [100] (A-axis), [010] (B-axis), and [001] (C-axis) directions, and are respectively called A-, B- and C-SLs. We define our frame of reference such that the polarization in oIII HfO_2 is along the C-axis (Fig. 2a). The A and B directions, both perpendicular to the polarization, can be distinguished by the orientation of the spacer layer, which lies parallel to the B-axis and perpendicular to the A-direction (Fig. 2b, c). Note that this frame of reference is uniquely defined for the oIII and m phases, while for the *t* phase the A and C directions (perpendicular to the 4-fold axis) are equivalent. Furthermore, the oIII and m SLs stacked along B can have the interface passing either through the polar layer (B_{pol}) or the spacer layer (B_{spc}), allowing for two inequivalent geometries (Fig. 2c, d respectively).

After each SL is completely relaxed, its formation energy is computed. For an X/Hf superlattice with equally thick XO_2 and HfO_2 layers, in some phase *p* (with *p* = oIII, oI, m, t), the formation energy per cation is defined as,

$$\triangle E^{SL}_{p-X,Hf} = E^{SL}_{p-X,Hf} - \frac{1}{2}\left(E^{Bulk}_{gs-XO_2} + E^{Bulk}_{gs-HfO_2}\right) \quad (1)$$

Here, $E^{SL}_{p-X,Hf}$ is the cohesive energy per cation of an X/Hf SL in phase *p*. Additionally, $E^{Bulk}_{gs-XO_2}$ and $E^{Bulk}_{gs-HfO_2}$ are the cohesive energies per cation of the fully relaxed pure compounds in their respective ground state. The second term on the right is then just the average of the bulk ground state cohesive energies of the pure compounds, and the difference with $E^{SL}_{p-X,Hf}$ gives the energy cost of producing the superlattice with respect to the separate bulks.

In order to discuss the relative stability of a particular superlattice with respect to the lowest-energy monoclinic (m) or distorted monoclinic (m') SL of the same composition, we introduce a quantity denoted "energy penalty", which is simply the difference in formation energy of the two SLs. More specifically, for an X/Hf SL in some phase *p*, the energy penalty with respect to its corresponding lowest-energy m (or m') SL is defined as,

$$\triangle E^{pen,SL}_{p-X,Hf} = \triangle E^{SL}_{p-X,Hf} - \triangle E^{SL}_{m-X,Hf} \quad (2)$$

Any SLs whose energy penalty is less than the energy of bulk polar oIII HfO_2 ($\triangle E^{pen,SL}_{p-X,Hf} < 64$ meV/cation, see Table 1) are more likely to support the ferroelectric state than bulk HfO_2 is. These SLs are hereafter referred to as 'competitive'. Furthermore, the SL's that satisfy the condition $\triangle E^{pen,SL}_{p-X,Hf} < 0$ correspond to a case where the phase *p* becomes the lowest energy state over the m or m' SLs. These SL's are hereafter referred to as 'favorable'. It should be noted that these lowest energy states are narrowly defined for the short-period 2/2 and 4/4 SLs, separately. We do not consider large-period SLs where the compounds of the SL are effectively separated, and lower energy phases can be obtained. In such structures, bulk effects are expected to dominate, while the effect of the interface becomes prominent in short-period SLs.

The formation energy of a particular phase of a particular SL is naturally the consequence of multiple, competing structural features and physical mechanisms. Two of these can be easily identified—the contributions from the bulk structure of each individual layer, and from the elastic constraints imposed at the interface of the two layers. Indeed, we can express the formation energy of an X/Hf SL in some phase *p* as the sum of a bulk contribution, an elastic contribution, and the remaining non-elastic contributions coming from the interfacial discontinuity:

$$\triangle E^{SL}_{p-X,Hf} = \triangle E^{Bulk\ avg}_{p-X,Hf} + \triangle E^{Elastic}_{p-X,Hf} + \triangle E^{Non-elastic}_{p-X,Hf} \quad (3)$$

The first term is an average of the energies of the pure compounds (XO_2 and HfO_2) in the phase *p*, defined with respect to their corresponding

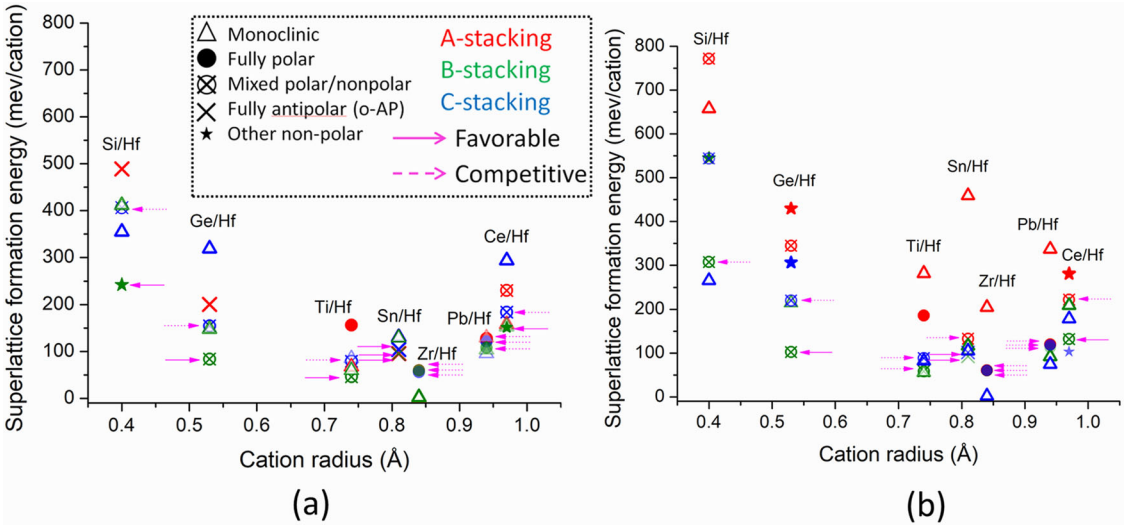

Fig. 3 | Superlattice formation energies. Formation energies of relevant SLs with monoclinic, polar, antipolar and mixed configurations, for (**a**) 2/2 and (**b**) 4/4 systems, plotted as a function of the radius of the non-Hf cation The dashed arrows identify phases in the competitive range, while the solid arrows indicate the favorable SLs.

ground state energies:

$$\triangle E^{\text{Bulk avg}}_{\text{p-X,Hf}} = \frac{1}{2}\left[\left(E^{\text{Bulk}}_{\text{p-XO}_2} - E^{\text{Bulk}}_{\text{gs-XO}_2}\right) + \left(E^{\text{Bulk}}_{\text{p-HfO}_2} - E^{\text{Bulk}}_{\text{gs-HfO}_2}\right)\right] \quad (4)$$

where $E^{\text{Bulk}}_{\text{p-XO}_2}$ and $E^{\text{Bulk}}_{\text{p-HfO}_2}$ are the cohesive energies of pure XO_2 and HfO_2 in phase p. The elastic contribution is instead given by

$$\triangle E^{\text{Elastic}}_{\text{p-X,Hf}} = \frac{1}{2}\left[\left(E^{\text{Const bulk}}_{\text{p-XO}_2} - E^{\text{Bulk}}_{\text{p-XO}_2}\right) + \left(E^{\text{Const bulk}}_{\text{p-HfO}_2} - E^{\text{Bulk}}_{\text{p-HfO}_2}\right)\right] \quad (5)$$

where $E^{\text{Const bulk}}_{\text{p-XO}_2}$ and $E^{\text{Const bulk}}_{\text{p-HfO}_2}$ are the cohesive energies of the pure compounds as obtained from a constrained relaxation, wherein we keep their in-plane lattice parameters strained to match those of the corresponding SLs. This term quantifies how much of the SL formation energy comes purely from the elastic straining of the pure compounds when they are put together in a heterostructure.

Finally, substituting (1), (3), and (4) into (2), we obtain the non-elastic component:

$$\triangle E^{\text{Non-elastic}}_{\text{p-X,Hf}} = E^{\text{SL}}_{\text{p-X,Hf}} - \frac{1}{2}\left(E^{\text{Const bulk}}_{\text{p-XO}_2} + E^{\text{Const bulk}}_{\text{p-HfO}_2}\right) \quad (6)$$

which is essentially a catch-all term that accounts for all effects due to the interface which are *not* explicitly elastic. These contributions, which are difficult to isolate, include chemical effects at the interface such as changes in bonding, as well as electrostatic effects due to depolarizing fields.

	Stackings:	A-SLs		B-SLs		C-SLs	
Composition	Thickness:	2/2	4/4	2/2	4/4	2/2	4/4
Zr/Hf	En. Penalty	58	56	59	56*	56	58*
	Polarization	0.56	0.56	0.56	0.56	0.55	0.55
	Structure	P/P	P/P	P/P	P/P	P/P	P/P
Pb/Hf	En. Penalty	32	45	12	38	26	44
	Polarization	0.47	0.47	0.53	0.54	0.52	0.51
	Structure	P/P	P/P	P/P	P/P	P/P	P/P
Sn/Hf	En. Penalty	-33	27	-33	-13*	-24	-4*
	Polarization	0	0.2	0	0	0	0
	Structure	A/A	A/P	A/A	A/A	A/A	A/A
Si/Hf	En. Penalty	134	506	-28	41	52	278
	Polarization	0	0.37	-0.1	0.21	0.26	0.28
	Structure	A/A	A/P	A/A	A/P	A/P	A/P
Ge/Hf	En. Penalty	56	130	-63	-112*	7	6*
	Polarization	0	0.23	0.1	0.2	0.22	0.24
	Structure	A/A	A/P	A/P	A/P	A/P	A/P
Ti/Hf	En. Penalty	97	129	-13*	45	20	32
	Polarization	0.69	0.68	0.16	0.21	0.36	0.38
	Structure	P/P	P/P	A/P	A/P	A/P	A/P
Ce/Hf	En. Penalty	77	44	-2	-46*	31*	-75*
	Polarization	0.2	0.23	0	0.18	0.23	0
	Structure	C/P	C/P	C/A	C/P	C/P	C/M

Fig. 4 | Structures, energies, polarizations of (initially) oIII SLs after relaxation. Formation energies are given in meV/cation, polarizations in C/m^2. Structures are classified as cubic (C), polar (P), antipolar (A) and monoclinic (M) for the X/Hf layers. Yellow shading indicates competitive superlattices, light green indicates favorable non-polar structures, dark green indicates favorable polar structures, and red indicates high energy phases. The structures with the asterisk are pictorially shown in the next section.

Energetics

The formation energies for some 2/2 and 4/4 SLs are shown in Fig. 3a, b, respectively, plotted as a function of the ionic radius of the X cation. Included are all the SLs relaxed starting from oIII and leading to various polar, nonpolar and mixed configurations, as well as the m SLs that are their competitors. Large variations in formation energies are observed for different stacking directions and compositions. Depending on these design parameters, the SLs starting from oIII end up in either fully polar (Fig. 3, '•'), fully antipolar (Fig. 3, '**X**'), or mixed polar/nonpolar (Fig. 3, '⊗') geometries with polar HfO_2 and approximately centrosymmetric XO_2 layers. Similarly, the initially monoclinic SLs generally relax to structures either close to the usual m phase or to a distorted m'-phase (both denoted by 'Δ' in Fig. 3), and in a few cases relaxes to entirely different phases (Fig. 3, '★'). Our main focus will naturally be on the low-laying SLs obtained from the oIII starting configuration, with a twofold interest: (a) the differences in their formation energies vis-a-vis the m SLs, and (b) the net polarization of the relaxed SLs. As it turns out, we can identify 23 orthorhombic SLs that are competitive with m SLs, i.e., an improvement over bulk oIII HfO_2 (Fig. 3, dashed arrows), as well as 4 polar and 7 antipolar configurations which are outright favorable (Fig. 3, bold arrows).

These details are summarized in Fig. 4, and further discussed in the subsequent sections. The formation energies of the various SLs grouped by composition, are given in Supplementary Tables 1–7, while the structures of the competitive and favorable SLs are given in VASP POSCAR format as supplementary data in the supplementary information file.

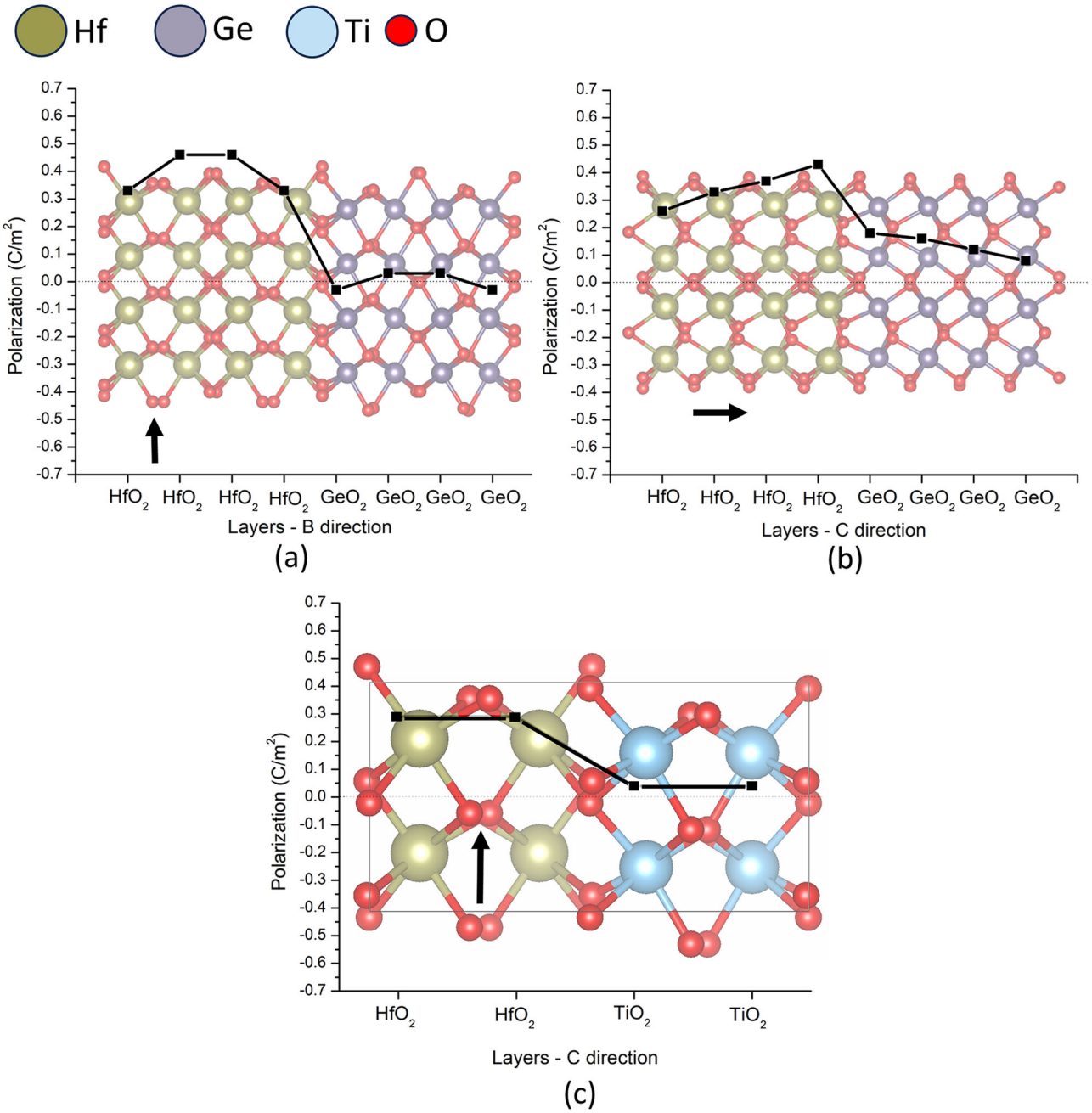

Fig. 5 | Structure and sublayer polarization of Ge/Hf and Ti/Hf mixed SLs. 4/4 Ge/Hf SL with (**a**) polarization in plane (B-SL) and (**b**) polarization out of plane (C-SL); (**c**) 2/2 Ti/Hf mixed SL with polarization in plane (B-SL). All structures were obtained by relaxing a fully oIII initial configuration.

Most promising polar superlattices

Of the various configurations outlined in Fig. 4, we first discuss the compositions where a polar solution is energetically favorable, as predicted for the mixed Ge/Hf, Ti/Hf and Ce/Hf superlattices.

The lowest energy configuration where a polar structure is stabilized is the B-oriented Ge/Hf system with 4/4 layer thicknesses (Fig. 5a). In this SL, the HfO_2 layer remains close to the bulk oIII phase with the polarization in the plane of the interface, while the GeO_2 layer tends towards its o-AP low energy bulk polymorph. The sublayer polarization peaks in the middle of the HfO_2 layer, and then drops sharply across the interface to approximately zero in the GeO_2 layer. The 2/2 Ge/Hf B-SLs are also similarly polar and favorable.

Another interesting structural feature is observed for the energetically very competitive 4/4 mixed oAP/oIII C-SL, which supports out-of-plane polarization across the polar/antipolar interface (Fig. 5b). In this case, the GeO_2 layer gets significantly polarized, so as to minimize the polarization discontinuity at the Ge/Hf interface and thus reduce the depolarizing fields. The polarization increases towards one interface and decreases at the other, suggesting the presence of bound charges at the interface. This is confirmed by the electronic density of states, which shows a decreasing band gap in the Ge/Hf C-SLs with increasing layer thickness (Supplementary Fig. 1); however, a metallic interfacial state is not present in the relatively short-period SLs investigated here.

Crucially, these low-energy o-AP/oIII SLs also have lower energy penalties than the corresponding fully antipolar oI'/oI SLs. Additionally, since GeO_2 has a rutile ground state, fully rutile structured SLs as well as mixed rutile/m and rutile/oIII SLs were also evaluated, and found to have formation energies higher than their o-AP/oIII counterparts (Supplementary Table 3).

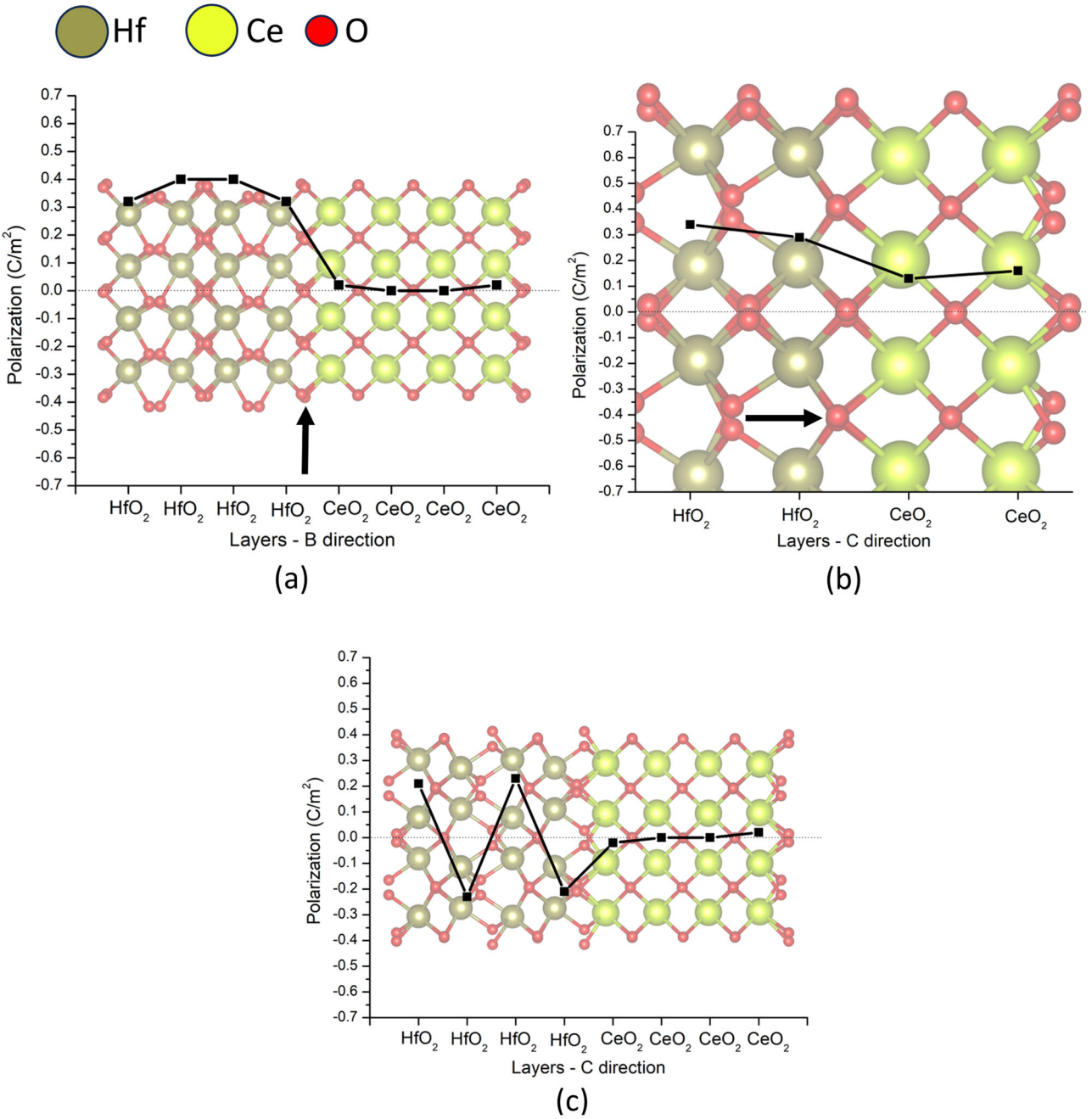

Fig. 6 | Structure and sublayer polarization of mixed Ce/Hf SLs. (**a**) 4/4 thickness and polarization in plane (B-SL); (**b**) 2/2 thickness and (**c**) 4/4 thickness, both with polarization out of plane (C-SL). All structures were obtained by relaxing a fully oIII initial configuration.

A further favorable configuration is obtained for the mixed Ti/Hf 2/2 o-AP/oIII B-SL (Fig. 5c) with a structure and polarization very similar to those of the corresponding Ge/Hf B-SLs. Additionally, both 2/2 and 4/4 mixed C-SLs and the 4/4 mixed B-SLs are energetically quite competitive against the m SLs and structurally similar to their Ge/Hf counterparts.

Finally, the Ce/Hf SLs also relax to mixed configurations, though of a different type. The peculiarities of this composition are preempted by the fact that Ce is the only lanthanide in a list of cations which are otherwise all group IV elements. The CeO_2 layer relaxes to a pseudocubic structure (similar to its bulk ground state) in most of the SLs. In the favorable 4/4 B-SLs, the HfO_2 layer remains in the polar oIII phase, with a sublayer polarization profile similar to the previously discussed mixed B-SLs (Fig. 6a). In the competitive 2/2 C-SL, the HfO_2 layer retains the polar structure while inducing a small polarization in the pseudocubic CeO_2 layer (Fig. 6b). However, in the 4/4 C-SL, the depolarizing field imposed by the CeO_2 layer becomes too strong, and the initially oIII HfO_2 layer relaxes into the m phase (Fig. 6c, Supplementary Fig. 2). This is accompanied by a significant reduction in formation energy, and this mixed cubic/monoclinic SL proves to be the lowest energy configuration of the 4/4 SLs. However, we find that this relaxation can be avoided – and an out-of-plane polarization of the HfO_2 layer retained—by reducing the thickness of the CeO_2 layer relative to the HfO_2 layer, as seen in the results for the 2/4 c/oIII Ce/Hf C-SL shown in Supplementary Fig. 3.

The least energetically viable composition for these mixed SLs is Si/Hf, where both the initially oIII and m SLs undergo large structural distortions on relaxation, and in several cases lead to high energy configurations that seem unlikely to occur in reality. Of all the compared oxides, the difference in cation radii (and lattice mismatch) is the largest for SiO_2 and HfO_2, leading to rather unstable systems. Nevertheless, the 4/4 B-SLs provide a competitive SL with a mixed o-AP/oIII configuration similar to Ge/Hf and Ti/Hf, with a similar sublayer polarization profile.

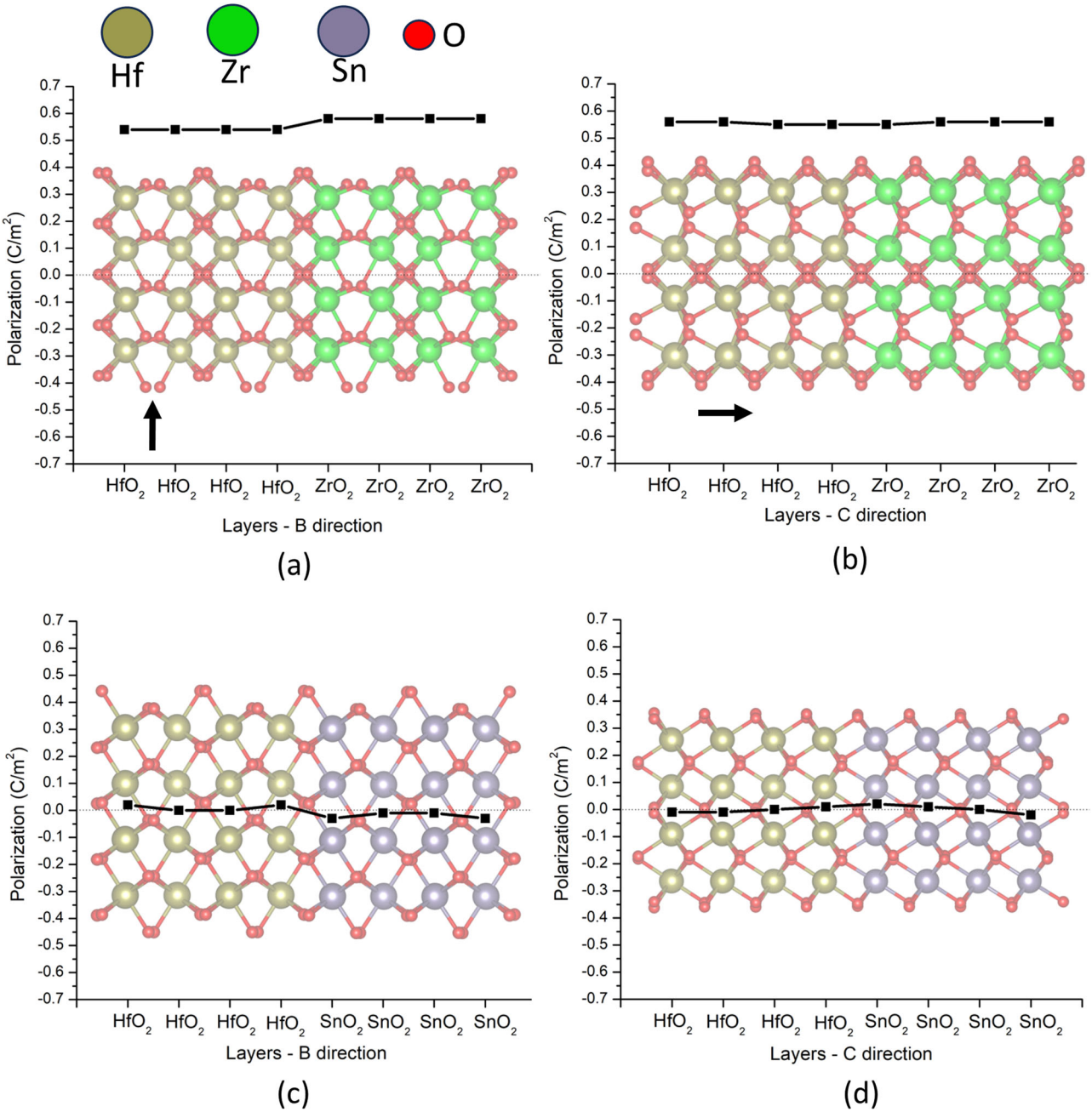

Fig. 7 | Structure and sublayer polarization of fully polar and fully antipolar SLs. 4/4 Zr/Hf oIII superlattices with (**a**) polarization in plane (B-SL) and (**b**) polarization out of plane (C-SL); and fully antipolar 4/4 Sn/Hf o-AP superlattices stacked along (**c**) B-, (**d**) C-directions. All structures were obtained by relaxing a fully oIII initial configuration.

Other promising polar and anti-polar superlattices

Energetically competitive structures are obtained for the fully polar Zr/Hf and Pb/Hf SLs, where the m ground state is less dominant than in bulk HfO_2. Here, the polarization is always close to that of bulk HfO_2 and largely uniform throughout the SL, with only a small kink at the interface (Fig. 7a, b). For all stacking directions and thicknesses, oIII SLs are energetically competitive, with Pb/Hf SLs having a somewhat reduced energy penalty compared to Zr/Hf. This is curious because unlike ZrO_2, PbO_2 does not have oIII or m local minima, but follows the HfO_2 layer, either into the oIII or the m phase, through a strain-induced relaxation (which we also obtain in the bulk compound when imposing SL-like strain constraints).

In sharp contrast to the previous examples, the Sn/Hf SLs are almost all favorable, but fully antipolar. Apart from the relatively higher energy 4/4 A-SL, which has a mixed structure, the other SLs starting from the oIII configurations all relax to a fully antipolar o-AP state. Here, SnO_2, which has no bulk oIII local minimum and a low energy o-AP phase, drives the HfO_2 layer into the o-AP structure through a strain-inudced relaxation (which, similar to PbO_2 described above, we can obtain in the bulk compound by imposing SL-like elastic constraints). Interestingly, this fully antipolar phase is more stable in the SLs than in the individual bulk oxides, and can offer a way to stabilize a potentially antiferroelectric state. However, SnO_2 has a rutile ground state, and the fully rutile Sn/Hf SLs have energies in the same range

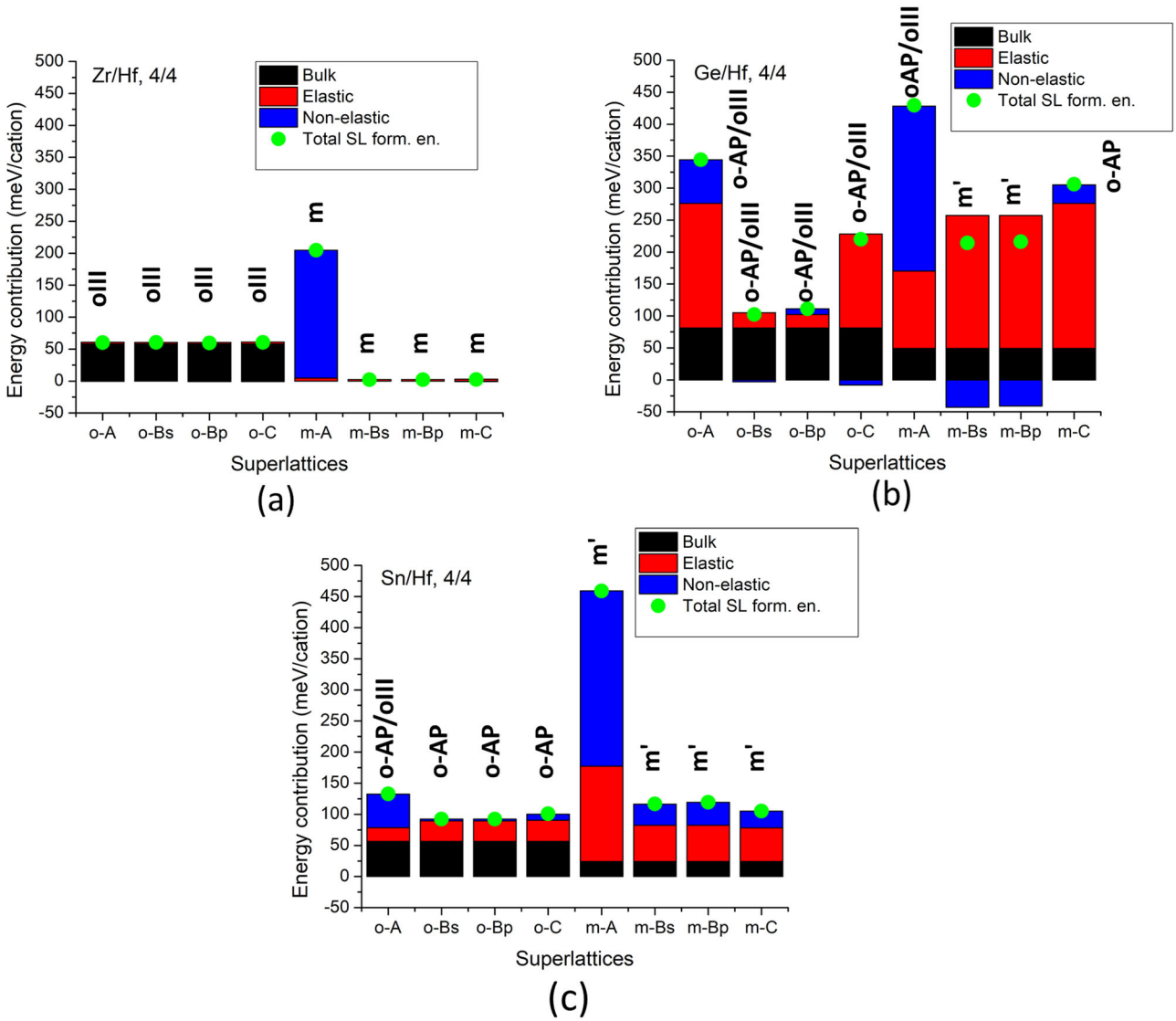

Fig. 8 | Formation energy decomposition. Contributions to the SL formation energies of Zr/Hf (**a**), Ge/Hf (**b**) and Sn/Hf (**c**) 4/4 SLs. The horizontal axis identifies the initial configurations – o (oIII) and m – as well as the stacking directions – A, C, Bs (B_{spc}) and Bp (B_{pol}) – while the vertical axis corresponds to the contributions to the formation energy from bulk (black), elastic (red) and non-elastic (blue) effects. The green dots show the total SL formation energy. The labels above each column identify the final structure of the respective SL after relaxation.

as the fully o-AP SLs (Supplementary Table 5), which suggests the possibility of competing phases in these materials.

Discussion

The results in the previous sections encompass a large variety of configurations, with seemingly uncorrelated behavior, arising in large part from the varied chemistry and complex polymorphism of these oxides. However, a closer look at the energetics of the various bulk polymophs, as well as the formation energy decomposition of the SLs, reveals a clear underlying mechanism responsible for stabilzing non-monoclinic structures.

We start with the homogenous Zr/Hf SLs, where both bulk oxides have monoclinic ground states and polar local minima of higher energy. Accordingly, the m SLs have lower formation energies than the polar SLs. Since the lattice mismatch between bulk HfO_2 and ZrO_2 (for both m and oIII phases) is small, the elastic penalties are negligible and the formation energy of the SLs are almost entirely dominated by the bulk contribution (Fig. 8a). Accordingly, these fully polar SLs still suffer from large energy penalties – the Zr/Hf oIII SLs have slightly lower energies than bulk oIII HfO_2 only because of the relatively low energy of bulk oIII ZrO_2.

To instead understand how we obtain favorable SLs, we inspect the representative case of the 4/4 o-AP/oIII Ge/Hf system. In this case, the polar phase with the lowest energy penalty corresponds to the stacking along the B-direction. As can be seen from the formation energy decomposition (Fig. 8b), this is because the elastic penalties for the orthorhombic SLs are very small for that particular stacking (in-plane polarization). This allows the low-energy coexistence of the polar oIII (in the HfO_2 layer) and antipolar o-AP (in the GeO_2 layer) structures in the mixed SLs (Fig. 5a). Instead, the (initially) monoclinic Ge/Hf SLs show large elastic contributions to the formation energy, with A-SLs and C-SLs actually relaxing into globally orthorhombic structures – mixed o-AP/oIII for the former and fully o-AP for the latter. This can be attributed to the absence of an m local minimum in bulk GeO_2, which ultimately makes the corresponding SLs either unviable or relatively high in energy (Fig. 8b). Indeed, we find a similar situation in TiO_2 and CeO_2, which suggests that a general necessary condition to stabilize the polar structure in the X/Hf SLs is the absence of monoclinic low-energy polymorph in the XO_2 layer. We should note here that the stability of these mixed o-AP/oIII SLs (as predicted for GeO_2, TiO_2 and CeO_2) is still quite remarkable, insofar as neither layer is in its bulk ground state. Rather, it

is the structural similarity between the o-AP and oIII structures (in contrast to the bulk monoclinic or tetragonal rutile ground states) that yields the o-AP/oIII mixed ground state for these systems.

The absence of a monoclinic polymorph for the XO_2 compound may also lead to non-polar (non-monoclinic) solutions. As an example, we may compare the *fully* antipolar Sn/Hf SLs with the mixed Ge/Hf SLs. Both GeO_2 and SnO_2 have similar polymorphism in the bulk (Table 1), which results in m-SLs having higher formation energies than the orthorhombic ones (Fig. 8c). However, constrained to the lattice parameters of the Sn/Hf SL, the HfO_2 layer becomes o-AP and, thus, a polar structure cannot be stabilized (Fig. 7c, d). Hence, we can conclude that the absence of a competing monoclinic phase is not a sufficient condition to stabilize polar SLs. Indeed, a second necessary condition is needed, namely, that the strain-state of the SLs supports the polar phase in at least the HfO_2 layer. Additionally, these strain induced relaxations prevent a simple correlation between the elastic penalties of the SLs and the average bulk elastic deformation energies of the two constituent oxides (see Supplementary Note 1).

Finally, it is worth noting that in the mixed nonpolar/polar SLs the lowest energy configurations are obtained with the polarization in the plane of the interface. This clearly resonates with well-known electrostatic effects in ferroelectric/dielectric superlattices (e.g., made by perovskite oxides $PbTiO_3$ and $SrTiO_3$) wherein states with in-plane polarization (and no accumulation of bound charges at the interface) are favored over those with an out-of-plane polarization (which inevitably yields interfacial bound charges and depolarizaing fields)[32]. This may also be the origin of the results obtained for the Ce/Hf C-SLs, where going from a 2/2 (Fig. 6b) to a 4/4 thickness (Fig. 6c) causes the HfO_2 layer to go into the m-phase and the polar structure to be lost. It is also interesting to note the case of the mixed 4/4 Ge/Hf C-SL, where the out-of-plane configuration seems somewhat more robust. To further test the stability of this C-oriented polar solution, we considered a SL where the HfO_2 layer displays a competing C-oriented polymorph, namely, the oI structure, which can be thought of as composed of anti-parallel domains of the polar oIII phase (Fig. 1d). As compared to oIII, this oI structure presents no net interfacial bound charges due to the interfacial discontinuity with the GeO_2 layer, which essentially cancels the depolarizing fields. However, the GeO_2 layer does not adapt to the oI structure of the HfO_2 layer and becomes distorted (oI', Supplementary Note 2). Accordingly, these SLs suffer larger energy penalties compared to the o-AP/oIII C-SL, and the mixed nonpolar/polar structure prevails.

The sensitivity of the SLs to elastic and electrostatic factors allows us to speculate on a further potential design parameter – the relative thickness of the individual layers. For example, while a 1:1 ratio clearly favors a fully antipolar phase in the Sn/Hf SLs, it can be reasonably expected that continuously increasing the thickness of the HfO_2 layer relative to SnO_2 will eventually lead to a polar structure. Hence, if we consider fully antipolar SLs just below this critical thickness ratio, we might be able to drive such systems into a polar phase by application of an electric field, which could provide us with an interesting family of materials to optimize antiferroelectric behavior. Similarly, increasing the relative thickness of the HfO_2 layer in the Ce/Hf C-SL will tend to favor structures with an out-of-plane polarization (see Supplementary Fig. 3), and whose stability – relative to non-polar states – can potentially be optimized. This may allow us to tune the energy barriers for ferroelectric switching and thus, potentially, control (reduce) the coercive fields while preserving a robust remnant polarization. At first glance it might appear that adding non-hafnia layers will inevitably result in a higher switching voltage, as we are introducing an extra dielectric layer (capacitor) in series with the ferroelectric (considering switching of an out-of-plane polarization). However, the extra layers may also allow us to reduce the value of the remnant polarization of the ferroelectric – and potentially induce a shallower energy landscape – which would result in a smaller coercive field. Hence, the superlattices offer us a non-trivial degree of freedom to optimize ferroelectric switching.

Finally, let us note that, despite the large number of systems studied, the present work should be considered neither exhaustive nor fully conclusive. Indeed, here we have only considered perfect, fully relaxed, monodomain, infinite crystal SLs stacked along specific crystallographic axes – by contrast, the effects of defects, epitaxial strain, domain formation, surfaces, and alternative stacking directions (including the possibility of different orientations for different layers[33]) have not been studied. Secondly, our work only addresses the thermodynamic stability of the discussed superlattices, without considering kinetic effects. Crucially, however, the mixed SLs discussed in this work are generally found to have energy costs lower than Zr/Hf SLs, which have already been synthesized and display promising properties. Hence, many of the SLs considered here – which show a better stability of the ferroelectric phase – are good candidates to improve over the Zr/Hf systems and further optimize performance.

In summary, the present study uses DFT calculations to study the structure and energetics of HfO_2-based simple oxide superlattices. Most remarkably, we identify several combinations presenting dominant ferroelectric phases. The necessary conditions favoring the stabilization of polar phases in these superlattices are twofold: (i) the absence of the monoclinic ground state in the non-HfO_2 oxide (which drives up the energy of corresponding monoclinic superlattices) and (ii) compatible elastic matching between the layers. The predicted ferroelectric solutions tend to present an in-plane polarization so as to minimize depolarizing fields. In addition, we also find other interesting ground states – e.g., of antipolar nature – that could provide a platform for the optimization of HfO_2-based antiferroelectrics.

Methods

First principles calculations

The first-principles calculations were performed with density functional theory using the plane-wave basis set as implemented in the Vienna ab-initio simulation package (VASP)[34–36]. The electron exchange correlation functional was approximated using the Perdew-Burke-Ernzerhof (PBE) form of the generalized gradient approximation (GGA) with PBEsol modification[37]. A cutoff of 600 eV was used for the expansion of the plane-waves. The valence states explicitly considered for the different elements are as follows: O – $2s^2$, $2p^4$; Ce – 5 s^2, $5p^6$, $4f^1$, $5d^1$, $6s^2$, Ge – $3d^{10}$, $4s^2$, $4p^2$; Pb – $5d^{10}$, $6s^2$, $6p^2$; Hf – $5p^6$, $5d^2$, $6s^2$; Si – $3s^2$, $3p^2$; Sn – $4d^{10}$, $5s^2$, $5p^2$; Ti – $3p^6$, $3d^2$, $4s^2$; Zr – $4s^2$, $4p^6$, $4d^2$, $5s^2$. For bulk structures, a 4x4x4 k-mesh was used to sample the Brillouin zone, with a proportional reduction to [4x4x2] and [4x4x1] along the stacking direction for the SLs. The structures were relaxed until the Hellmann-Feynman forces on each atom fell below 0.01 eV/Å.

VASPKIT[38] and FINDSYM[39] were used for postprocessing, while VESTA[40] was used for structure visualization.

Polarization calculation

The layer-by-layer polarization for the SLs was computed as the product of the nominal charges (+4 for cations, -2 for oxygen), and the displacements of the ions with respect to the high symmetry cubic fluorite parent structure (Fm-3m), normalized by the volume of half a single unit cell (i.e., a 'sub-layer'). This consists of a lower limit for the polarization. The polarization of the bulk oIII phase of HfO_2 with Born effective charges instead of nominal charges is calculated for comparison in Supplementary Note S3, and shows an increase of ~25%.

Data availability

The authors declare that the data supporting the findings of this study are available within the paper, and its supplementary information files. Further data sets generated during the current study may be obtained from the corresponding author on reasonable request.

Received: 10 January 2024; Accepted: 4 July 2024;
Published online: 16 July 2024

References

1. Schroeder, U., Park, M. H., Mikolajick, T. & Hwang, C. S. The fundamentals and applications of ferroelectric HfO2. *Nat. Rev. Mater.* **7**, 653–669 (2022).

2. Böscke, T. S., Müller, J., Bräuhaus, D., Schröder, U. & Böttger, U. Ferroelectricity in hafnium oxide thin films. *Appl. Phys. Lett.* **99**, 102903 (2011).
3. Delodovici, F., Barone, P. & Picozzi, S. Trilinear-coupling-driven ferroelectricity in HfO2. *Phys. Rev. Mater.* **5**, 064405 (2021).
4. Zhou, S., Zhang, J. & Rappe, A. M. Strain-induced antipolar phase in hafnia stabilizes robust thin-film ferroelectricity. *Sci. Adv.* **8**, 47 (2022).
5. Raeliarijaona, A. & Cohen, R. E. Hafnia HfO2 is a proper ferroelectric. *Phys. Rev. B* **108**, 094109 (2023).
6. Aramberri, H. & Íñiguez, J. Theoretical approach to ferroelectricity in hafnia and related materials. *Commun. Mater.* **4**, 95 (2023).
7. Schroeder, U. et al. Temperature-dependent phase transitions in HfxZr1-xO2 mixed oxides: indications of a proper ferroelectric material. *Adv. Electron Mater.* **8**, 2200265 (2022).
8. Dutta, S. et al. Piezoelectricity in hafnia. *Nat. Commun.* **12**, 7301 (2021).
9. Liu, J., Liu, S., Liu, L. H., Hanrahan, B. & Pantelides, S. T. Origin of pyroelectricity in ferroelectric HfO2. *Phys. Rev. Appl.* **12**, 034032 (2019).
10. Liu, J., Liu, S., Yang, J. Y. & Liu, L. Electric auxetic effect in piezoelectrics. *Phys. Rev. Lett.* **125**, 197601 (2020).
11. Wu, Y. et al. Unconventional polarization-switching mechanism in ferroelectrics and its implications. *Phys. Rev. Lett.* **131**, 226802 (2023).
12. Qi, Y., Reyes-Lillo, S. E. & Rabe, K. M. 'Double-path' ferroelectrics and the sign of the piezoelectric response, Preprint at arXiv:2204.06999 [cond-mat.mtrl-sci], (2022).
13. Materlik, R., Kunneth, C. & Kersch, A. The origin of ferroelectricity in Hf1-xZrxO2: a computational investigation and a surface energy model. *J. Appl. Phys.* **117**, 134109 (2015).
14. Yuan, J. H. et al. Ferroelectricity in HfO2 from a coordination number perspective. *Chem. Mater.* **35**, 94–103 (2023).
15. Schroeder, U., Hwang, C. S., Funakubo, H., *Ferroelectricity in Doped Hafnium Oxide: Materials, Properties and Devices*., Woodhead, ISBN: 978-0-08-102430-0 (2019).
16. Park, M. H., Lee, Y. H. & Hwang, C. S. Understanding ferroelectric phase formation in doped HfO2 thin films based on classical nucleation theory. *Nanoscale* **11**, 19477–19487 (2019).
17. Xu, X. et al. Kinetically stabilized ferroelectricity in bulk single-crystalline HfO2:Y. *Nat. Mater.* **20**, 826–832 (2021).
18. Materano, M. et al. Interplay between oxygen defects and dopants: effect on structure and performance of HfO2-based ferroelectrics. *Inorg. Chem. Front.* **8**, 2650–2672 (2021).
19. Zhu, T., Deng, S. & Liu, S. Epitaxial ferroelectric hafnia stabilized by symmetry constraints. *Phys. Rev. B* **108**, L060102 (2023).
20. Dutta, S., Aramberri, H., Schenk, T. & Íñiguez, J. Effect of Dopant ordering on the stability of ferroelectric hafnia. *Phys. Status Solidi Rapid Res. Lett.* **14**, 2000047 (2020).
21. Lehninger, D. et al. Ferroelectric [HfO_2/ZrO_2] superlattices with enhanced polarization, tailored coercive field, and improved high temperature reliability. *Adv. Phys. Res.* **2**, 2200108 (2023).
22. Liang, Y. K. et al. ZrO2-HfO2Superlattice ferroelectric capacitors with optimized annealing to achieve extremely high polarization stability. *IEEE Electron Device Lett.* **43**, 1451–1454 (2022).
23. Cheema, S. S. et al. Ultrathin ferroic HfO2–ZrO2 superlattice gate stack for advanced transistors. *Nature* **604**, 65–71 (2022).
24. Bai, N. et al. Designing wake-up free ferroelectric capacitors based on the HfO2/ZrO2 superlattice structure. *Adv. Electron Mater.* **9**, 2200737 (2023).
25. Park, M. H. et al. A comprehensive study on the mechanism of ferroelectric phase formation in hafnia-zirconia nanolaminates and superlattices. *Appl. Phys. Rev.* **6**, 041403 (2019).
26. Gong, Z. et al. Physical origin of the endurance improvement for HfO2-ZrO2 superlattice ferroelectric film. *Appl Phys. Lett.* **121**, 242901 (2022).
27. Aamlid, S. S. et al. Phase stability of entropy stabilized oxides with the α-PbO2 structure. *Commun. Mater.* **4**, 45 (2023).
28. Zhu, T. & Gao, S. P. The stability, electronic structure, and optical property of tio 2 polymorphs. *J. Phys. Chem. C* **118**, 11385–11396 (2014).
29. Deringer, V. L., Lumeij, M., Stoffel, R. P. & Dronskowski, R. Ab initio study of the high-temperature phase transition in crystalline GeO2. *J. Comput. Chem.* **34**, 2320–2326 (2013).
30. Mazumder, J. T., Mayengbam, R. & Tripathy, S. K. Theoretical investigation on structural, electronic, optical and elastic properties of TiO2, SnO2, ZrO2 and HfO2 using SCAN meta-GGA functional: a DFT study. *Mater. Chem. Phys.* **254**, 123474 (2020).
31. Coh, S. & Vanderbilt, D. Structural stability and lattice dynamics of SiO2 cristobalite. *Phys. Rev. B* **78**, 054117 (2008).
32. Junquera, J. et al. Topological phases in polar oxide nanostructures. *Rev. Mod. Phys.* **95**, 025001 (2023).
33. Zhao, G. D., Liu, X., Ren, W., Zhu, X. & Yu, S. Symmetry of ferroelectric switching and domain walls in hafnium dioxide. *Phys. Rev. B* **106**, 064104 (2022).
34. Kresse, G. & Furthmüller, J. Efficiency of ab-initio total energy calculations for metals and semiconductors using a plane-wave basis set. *Comput Mater. Sci.* **6**, 15–50 (1996).
35. Kresse, G. & Furthmüller, J. Efficient iterative schemes for ab initio total-energy calculations using a plane-wave basis set. *Phys. Rev. B* **54**, 11169–11186 (1996).
36. Kresse, G. & Hafner, J. Ab initio molecular-dynamics simulation of the liquid-metalamorphous- semiconductor transition in germanium. *Phys. Rev. B* **49**, 14251–14269 (1994).
37. Terentjev, A. V., Constantin, L. A. & Pitarke, J. M. Dispersion-corrected PBEsol exchange-correlation functional. *Phys. Rev. B* **98**, 1–12 (2018).
38. Wang, V., Xu, N., Liu, J. C., Tang, G. & Geng, W. T. VASPKIT: a user-friendly interface facilitating high-throughput computing and analysis using VASP code. *Comput. Phys. Commun.* **267**, 108033 (2021).
39. Stokes, H. T. & Hatch, D. M. FINDSYM: Program for identifying the space-group symmetry of a crystal. *J. Appl. Crystallogr.* **38**, 237–238 (2005).
40. Momma, K. & Izumi, F. VESTA 3 for three-dimensional visualization of crystal, volumetric and morphology data. *J. Appl. Crystallogr.* **44**, 1272–1276 (2011).
41. Shannon, R. D. Revised effective ionic radii and systematic studies of interatomie distances in halides and chaleogenides. *Acta Cryst.* **32**, 751–767 (1976).

Acknowledgements

BM would like to thank Dr. Hugo Aramberri for many useful discussions. This work was supported by the Luxembourg National Research Fund though grant Nos. INTER/NOW/20/15079143/TRICOLOR.

Author contributions

BM was responsible for making the calculations, interpreting and analysing the results and writing the manuscript. NSF was responsible for analyzing the results and editing the manuscript. JÍ-G was responsible for conceiving and supervising the study, analyzing the results and editing the manuscript.

Competing interests

The authors declare no competing interests.

Additional information

Supplementary information The online version contains supplementary material available at https://doi.org/10.1038/s41524-024-01344-0.

Correspondence and requests for materials should be addressed to Binayak Mukherjee or Jorge. Íñiguez-González.